Pergamon

Int. J. Heat Mass Transfer. Vol. 41, Nos 8–9, pp. 1013–1024, 1998

Printed in Great Britain
0017–9310/98 $19.00+0.00

PII: S0017–9310(97)00215–9

Heat balance over the fluid-dynamic boundary layer of a circulating fluidized bed furnace

CLAES BREITHOLTZ and BO LECKNER*

Department of Energy Conversion, Chalmers University of Technology, S-412 96 Gothenburg, Sweden

(*Received* 14 *October* 1996 *and in final form* 15 *July* 1997)

Abstract—A heat balance over the fluid-dynamic boundary layer of a circulating fluidized bed furnace has been formulated in order to calculate the heat transfer to the walls. The convective heat transfer is related to a horizontal particle flow from the core to the wall region, and an additive radiative heat transfer constituent is calculated for the particulate medium. An empirical description of the vertical distribution of solids and the transversal temperature profile are needed for the evaluation. The calculated heat transfer coefficients were compared with measurements in three commercial boilers and the deviation was less than 40%, which is in the same order as the uncertainty of the experimental data. © 1997 Elsevier Science Ltd.

INTRODUCTION

The temperature in a circulating fluidized bed (CFB) furnace is generally controlled by heat transfer to the membrane-tube walls of the furnace. The approaches chosen for prediction of the heat transfer can be divided into two groups: correlations and mechanistic models.

The model of Werderman and Werther [1] estimates the convective heat transfer by a curve-fit correlation. An additive radiative heat transfer component is calculated for a porous medium with a known temperature profile. Wirth [2] bases a correlation of the convective component on dimensional analysis, approximates the radiation to that between two infinite walls and weights the components together in an arbitrary way. Finally, Andersson [3] correlates the total heat transfer. The correlations reveal that particle concentration is the most important heat transfer parameter, but the underlying mechanisms are not explained. Even if the model of Wirth considers phenomena in the fluid-dynamic boundary-layer (FBL), the model does not account for the formation of the FBL. Hence, this group of models can hardly be extrapolated.

The mechanistic models, on the other hand, are founded on assumptions about the fluid-dynamics of the CFB furnace. The majority of the models, e.g. [4–7], are related to the penetration theory. It is assumed that packets of particles enter the FBL, leave some of their heat and return to the core. To use these models, information about the fluid-dynamics at the wall is required [8]:

- particle concentration in the clusters;
- fraction of wall covered by clusters;
- residence time of clusters at the wall;
- thickness of the gas-layer between particles and wall;
- heat transfer coefficient of the dilute phase.

However, the concept of a two-phase flow pattern consisting of clusters and a dilute phase between them is not an unambiguous description of the FBL [9].

Some results concerning the above list of items have been published. The residence length of particles at the wall has been measured [10] indicating lengths below 1 m in a 9.2 m high and 0.15 m wide CFB test rig. In the same test rig the residence length was used as a fitting parameter [7] and a length of 4 m was found. Consequently, there are no consistent data about residence length. Also measurements of the thickness of the gas-layer between particles and wall are not in general agreement. In one investigation [11] the thickness was found to be in the order of 1 mm, corresponding to about 10 particle diameters, whereas in another [8] this thickness was determined to 0.1–0.4 mm. The discrepancy between these measurements cannot be explained. Consequently, these results need to be completed by further investigations before they can be generalized.

It can be stated as a conclusion that the present knowledge on the local fluid-dynamics is not sufficient for the establishment of generally valid models which can be extrapolated beyond the range of underlying data. On the other hand, the global flow pattern described by a core-annulus structure is accepted for laboratory-scale test rigs as well as for CFB furnaces. Such a flow pattern means that particles are separated from the up-flow in the core of the riser to an FBL of descending particles, which is called annulus in chemical reactor applications (the reactors usually have a circular cross-section) or wall-layers in the case

† Author to whom correspondence should be addressed.

NOMENCLATURE

A	area of a radiating slab element [m^2]
$\mathbf{A}$	matrix of the system of differential equations of the two-flux model
a	parameters in the correlation of the horizontal temperature profile
b	parameters in the correlation of the normalized horizontal particle distribution
C	projected area of the particles in a unit volume [m^{-1}]
c	two-dimensional distribution of particle concentration
c_p	heat capacity, [J kg^{-1} $°C^{-1}$]
D	side width of a corresponding square cross-section of the furnace [m]
d_p	Sauter mean diameter of bed material [m]
E	total emissive power [W m^{-2}]
G	mass flux [kg m^{-2}]
H	height of the furnace, counted from the air distributor level [m]
I	radiation intensity [W m^{-2} sr^{-1}]
J	radiosity [W m^{-2} sr^{-1}]
K	decay constant of the volumetric particle concentration in the transport zone [m^{-1}]
k	net deposition coefficient [m s^{-1}]
m	mass of the particles in the transport zone [kg]
Q	heat flux [W]
s	inhomogeneous part of the system of differential equations of the two-flux model [W m^{-2} sr^{-1}]
T	temperature [°C or K]
u	superficial velocity [m s^{-1}]
v	particle velocity [m s^{-1}]
x	distance from the wall or the fin [m]
z	height above the air distributor [m].

Greek symbols

α	heat transfer coefficient [W m^{-2} $°C^{-1}$]
β	constants in the solution of the two flux model [W m^{-2} sr^{-1}]
δ	thickness of the fluid-dynamic boundary-layer [m]
$\Delta\varepsilon$	compensation for spectral overlap of water vapor and carbon dioxide
ε	emissivity
γ	reduced horizontal distribution of particle concentration
η	backmixing fraction of the furnace exit, $1-\eta$ is the separation efficiency of the furnace exit
κ	thickness of a particle cloud [m]
μ	$\cos(\varphi)$
ξ	transmittance
ρ	density [kg m^{-3}]
σ	Stefan–Boltzmann's constant, 5.67×10^{-8} [W m^{-2} K^{-4}]
τ	optical depth
φ	polar angle between directions of observation and propagation [rad]
ψ	cross-sectional average volumetric particle concentration.

Subscripts

H_2O	water vapor
CO_2	carbon dioxide
$-$	negative x-direction
$+$	positive x-direction
0	end of the heat transfer surface
b	black body
c	core
conv	convective
cup	cup-mixing average
d	direct
eff	effective
fbl	fluid-dynamic boundary-layer
g	gas
hom	homogeneous solution
in	flux into the FBL
out	flux out from the FBL
p	particle
part	particular solution
rad	radiative
s	gas-particle suspension
ss	single-scattering
t	terminal
ts	two-way scattering
tot	total
w	wall
x	in x direction
φ	directional.

of plane walls. In a tall and narrow riser (large height to diameter ratio) the flow is fully developed: the suspension density is almost invariant with height and the flow into the wall-layer is equal to the flow out of the layer. In combustors (having a small height to diameter ratio) the flow is developing: there is a net flow of particles predominantly from the core to the wall-layers also in the transport-zone, where the heat transfer surfaces are located, and a corresponding fall-off in particle concentration with height. The vertical fall-off in concentration can be readily calculated from pressure drop measurements and corresponds to the

net flux of particles to the wall. This flux of particles carries heat to the wall. The heat transport from the core of the transport zone to the wall may be divided into three steps: from the core to the FBL, through the FBL and from the FBL to the wall. The model proposed is based on the time-average global flow pattern of particles to estimate the average heat transfer to the wall of the combustion chamber, expressed as a projected surface.

HEAT TRANSFER MODEL

The heat balance, illustrated in Fig. 1(a) and (b), comprises five terms: the heat transported by the net flow of particles from the core to the FBL and by particles re-entering the bottom bed, radiation from the core to the FBL and radiation from the FBL to the core. The fifth term, the heat received by the wall, becomes

$$Q_w = Q_{conv,in} - Q_{conv,out} + Q_{rad,in} - Q_{rad,out}. \quad (1)$$

Fluid-dynamics

A description of the particle concentration and particle flow is needed before the heat fluxes can be determined. The particle volume concentration $c(x, z)$ can be expressed by

$$c(x, z) = \gamma(x)\psi(z) \quad (2)$$

where $\psi(z)$ is the axial distribution of the cross-section average volumetric concentration of particles, usually obtained by pressure drop measurements. It can be described by an exponential decay in the transport zone [12],

$$\psi(z) = \psi(H)\exp[K(H-z)] \quad (3)$$

where $\psi(H)$ is the concentration at the top. The transversal particle concentration is higher close to the walls than in the center of the bed [13, 14]. The transversal particle concentration profile, $\gamma(x)$, is expressed as a distribution around the cross-sectional average value

$$\gamma(x) = b_0 + b_1 \exp[-b_2 x/D] \quad (4)$$

where b_0, b_1 and b_2 are coefficients to be determined empirically. The form of this function was chosen to simplify the mathematical manipulation. The small regions with higher concentrations in the corners of the furnace are neglected by assuming the con-

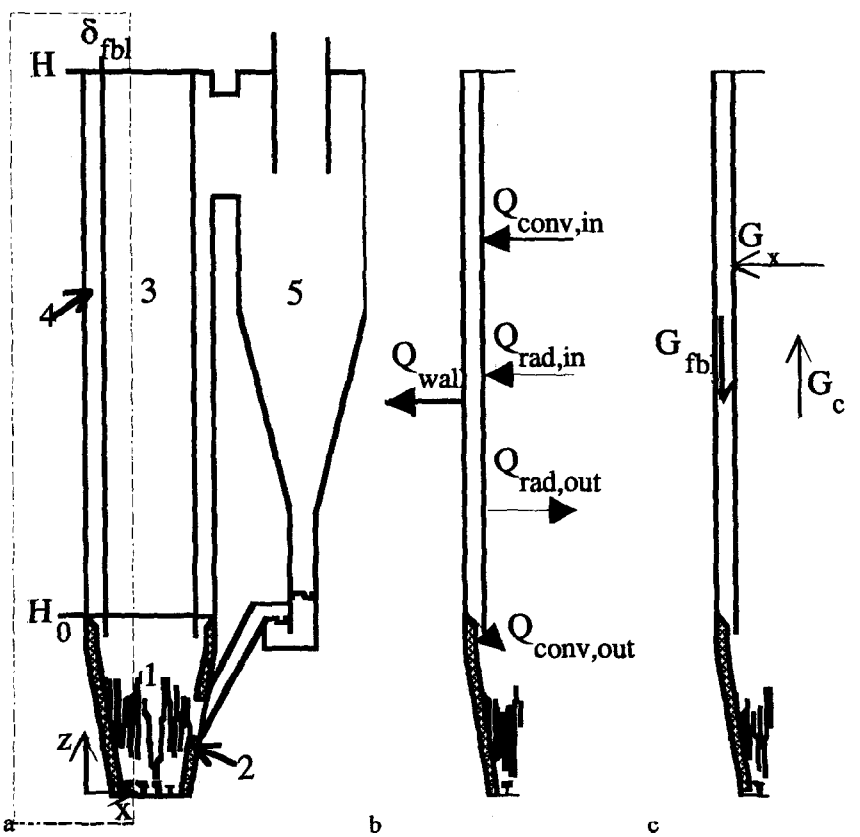

Fig. 1. A CFB with a control volume (a) showing a wall and a wall-layer over which heat (b) and mass balances (c) are made. The balance is shown for one wall but similar balances are made for the other (almost) identical three walls. (1) Refractory lined bottom zone; (2) refractory; (3) transport zone; (4) wall-layer; and (5) cyclone.

centration to be dependent only on the distance from the walls. This is a reasonable assumption in boilers where the extension of the corner regions is small compared to the width of the wall. The cross-sectional average of eqn (4), should be equal to unity in a square cross-section with the side width D

$$\int_0^{D/2} \gamma(x)(D-2x)\,dx \Big/ \int_0^{D/2} (D-2x)\,dx = 4\left(\frac{b_1}{b_2}+\frac{b_0}{4}+\frac{2b_1}{b_2^2}\left(\exp\left[-\frac{b_2}{2}\right]-1\right)\right)=1. \quad (5)$$

In analogy with eqn (5) average values of γ for the FBL, γ_{fbl}, and for the core, γ_c, are obtained by integration over the FBL and the core,

$$\gamma_{fbl} = \int_0^{\delta} \gamma(x)(D-2x)\,dx \Big/ \int_0^{\delta} (D-2x)\,dx \quad (6a)$$

$$\gamma_c = \int_{\delta}^{D/2} \gamma(x)(D-2x)\,dx \Big/ \int_{\delta}^{D/2} (D-2x)\,dx \quad (6b)$$

yielding

$$4((\delta/D-(\delta/D)^2)\gamma_{fbl}+(1/2-\delta/D)^2\gamma_c)=1. \quad (7)$$

Three main components of the global particle flow pattern [15] as indicated in Fig. 1(c), will be described here: an up-flow in the core $G_c(z)$, a net flow $G_x(z)$ from the core to the FBL, and a down-flow $G_{fbl}(z)$ in the FBL.

In the core, the particles flow under dilute conditions, and the particle velocity is assumed to be equal to the difference between the fluidization velocity and the terminal velocity of a single particle. The up-flow of particles per unit area in the core is then expressed as the product of the particle velocity $(u-v_t)$ and the suspension density in the core,

$$G_c(z) = (u-v_t)\rho_p\gamma_c\psi(H)\exp[K(H-z)]. \quad (8)$$

The particle flow is zero for fluidization velocities lower than the terminal velocity. The net particle flow into the FBL is expressed as the product of a net deposition coefficient k and the suspension density in the core [15, 16],

$$G_x(z) = k\rho_p\gamma_c\psi(H)\exp[K(H-z)]. \quad (9)$$

If all back-mixing of particles in the transport zone from H_0 to H takes place in the FBL with a constant k, then the in-flow to the wall layer should be equal to the change of the flow in the core,

$$4(D-2\delta)G_x(z) = -(D-2\delta)^2\frac{dG_c(z)}{dz}. \quad (10)$$

A relation between the decay constant K and the net deposition coefficient k is obtained from eqn (10) by assuming that $(D-2\delta)\approx D$,

$$k = KD(u-v_t)/4. \quad (11)$$

The down-flow in the FBL is the sum of particles, which fall down from the top of the furnace, and the net transversal particle flow integrated from the furnace top. The initial down-flow into the FBL, $G_{fbl}(H)$, is described by the fraction η of the flow in the core which is not carried away into the cyclone by the gas but remains in the furnace. This quantity is obtained from the mass balance at the top of the furnace where $z = H$,

$$4D\delta G_{fbl}(H) = -D^2\eta G_c(H). \quad (12)$$

$G_c(H)$ is given by eqn (8). The expression for the down-flow is the sum of the initial down-flow and the accumulated net in-flow from the core

$$G_{fbl}(z) = G_{fbl}(H)+\frac{1}{\delta}\int_H^z G_x(z)\,dz = -\left(\frac{D\eta(u-v_t)}{4}+\frac{k}{K}[\exp[K(H-z)]-1]\right)\times\frac{\rho_p\gamma_c\psi(H)}{\delta}. \quad (13)$$

The flow of particles leaving the FBL is obtained from eqn (13) with $z = H_0$.

Particle convection

At a load above, say 50% for most designs, the horizontal temperature profile of a CFB combustion chamber is almost independent of height and can be fitted by the expression,

$$T(x) = T_c - a_1\exp[-a_2x/D] \quad (14)$$

where the core temperature T_c is given and a_1 and a_2 are empirical constants. The total mass of particle transferred to the FBL is known by eqn (13), and the corresponding heat flow becomes,

$$Q_{conv,in} = -4D\delta G_{fbl}(H_0)T_c c_{p,p} \quad (15)$$

where $c_{p,p}$ is the specific heat of the particles. The heat of the particles leaving the FBL is calculated in a similar way by assuming that the cup-mixing temperature of the FBL is

$$T_{cup} = \int_0^{\delta} T(x)\gamma(x)\,dx \Big/ \int_0^{\delta}\gamma(x)\,dx = \left\{\frac{b_0T_c\delta}{D}-\frac{a_1b_1}{a_2+b_2}\left(1-\exp\left[-\frac{(a_2+b_2)\delta}{D}\right]\right)+\frac{T_cb_1}{b_2}\left(1-\exp\left[-\frac{b_2\delta}{D}\right]\right)-\frac{a_1b_0}{a_2}\left(1-\exp\left[-\frac{a_2\delta}{D}\right]\right)\right\}\Big/\left\{\frac{b_0\delta}{D}+\frac{b_1}{b_2}\left(1-\exp\left[-\frac{b_2\delta}{D}\right]\right)\right\} \quad (16)$$

where the particle velocity was assumed constant over the horizontal cross-section of the FBL.

Similar to eqn (15) the heat leaving the FBL now becomes

$$Q_{\text{conv,out}} = -4D\delta G_{\text{fbl}}(H_0)T_{\text{cup}}c_{\text{p,p}}. \quad (17)$$

According to its definition the average convective heat transfer coefficient is

$$\alpha_{\text{conv}} = (Q_{\text{conv,in}} - Q_{\text{conv,out}})/(4D(H-H_0)(T_c - T_w)) \quad (18)$$

and with eqns (15) and (17) this can be expressed as

$$\alpha_{\text{conv}} = -\delta G_{\text{fbl}}(H_0)c_{\text{p,p}}(T_c - T_{\text{cup}})/((H-H_0)(T_c - T_w)). \quad (19)$$

Thermal radiation

Heat is also transferred by radiation from the core to the walls and back from the FBL to the core. The radiation from the core towards the flat walls is

$$Q_{\text{rad in}} = 4D(H-H_0)\varepsilon_c\sigma T_c^4. \quad (20)$$

Assuming grey radiation, the emissivity of the core ε_c can be expressed according to the law of transmittance by the product of the transmittance of the gas $(1-\varepsilon_g)$ and that of the particle suspension

$$(1-\varepsilon_{\text{eff}}),\ \varepsilon_c = 1-(1-\varepsilon_g)(1-\varepsilon_{\text{eff}}) = \varepsilon_g + \varepsilon_{\text{eff}} - \varepsilon_g\varepsilon_{\text{eff}}. \quad (21)$$

The gas emissivity is calculated for the average composition of the combustion gas [17].

$$\varepsilon_g = \varepsilon_{H_2O} + \varepsilon_{CO_2} - \Delta\varepsilon. \quad (22)$$

The emissivity, ε_{eff}, of an isothermal particle suspension with constant concentration has been evaluated according to the two-flux approximation of radiative transfer in Appendix A. The result is for a given particle emissivity ε_p,

$$\varepsilon_{\text{eff}} = 2\varepsilon_p^{1/2}\left(1-\exp\left[-\varepsilon_p^{1/2}\frac{3\psi(z)\gamma_c}{d_p}x\right]\right)\Big/ \left(1+\varepsilon_p^{1/2}+(1-\varepsilon_p^{1/2})\exp\left[-\varepsilon_p^{1/2}\frac{3\psi(z)\gamma_c}{d_p}x\right]\right). \quad (23)$$

This relationship is shown in Fig. A1 as a function of the optical depth τ defined as the projected area of the particles in the volume

$$\tau = \int_{x_1}^{x_2}\frac{3}{2}\frac{c(x,z)}{d_p}\,dx. \quad (24)$$

In the limiting case $\tau \to \infty$ the emissivity of the particle suspension becomes

$$\varepsilon_{\text{eff}}(\tau\to\infty) = 2\varepsilon_p^{1/2}/(1+\varepsilon_p^{1/2}). \quad (25)$$

As seen from Fig. A1 this takes place already for $\tau > 3$.

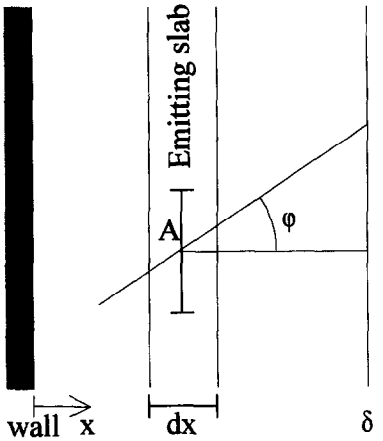

Fig. 2. Radiation from a slab in the FBL with the thickness dx in the direction φ from the normal of the slab.

The radiation from the FBL to the core is more complex because of the temperature variation in the coinciding thermal boundary layer and the contribution of the wall. A sufficiently thin slab with the thickness dx in the wall-layer can be considered isothermal and having a constant particle concentration. The intensity emitted in any direction φ (Fig. 2) to the normal of the slab is proportional to the projected area of the particles in a plane normal to the direction of radiation. The area of the slab, A, is scaled with a factor $\mu = \cos(\varphi)$ to get the projected area $(A\mu)$. The distance through the slab is accordingly scaled with the distance $1/\mu$, Fig. 2. The directional effects, a smaller area and a longer distance through the slab, cancel and the radiation is isotropic.

$$I(x,z) = \frac{\varepsilon_p\sigma T^4}{\pi}d\tau(x,z). \quad (26)$$

Assuming scattering to be directed forwards or backwards, as described in Appendix B, the directional transmittance at a certain level z from a horizontal position x to the boundary of the wall-layer at the position $x = \delta$ can be expressed as

$$\xi_{\text{ts},\varphi}(x,\delta) = \exp\left[-\int_x^\delta\left(\frac{1+\varepsilon_p}{2}\right)\frac{d\tau(x',z)}{\mu}\right]. \quad (27)$$

Integration over all directions and slabs in the wall-layer yields the emissive power,

$$E_+(\delta,z) = \int_0^\delta 2\varepsilon_p\sigma T(x)^4\int_0^1\xi_{\text{ts},\varphi}(x,\delta)\,d\mu\,d\tau(x,z). \quad (28)$$

The radiation from a diffusely reflecting and emitting wall, the radiosity, consists of emission from the wall and reflection of incident radiation,

$$J(z) = \varepsilon_w\sigma T_w^4 + (1-\varepsilon_w)E_-(0,z). \quad (29)$$

The incident radiation is calculated in analogy to eqn (28)

$$E_-(0,z) = \int_0^{\delta} 2\varepsilon_p \sigma T(x)^4 \int_0^1 \xi_{ts,\varphi}(0,x)\,d\mu\,d\tau(z,x) + \varepsilon_c \sigma T_c^4 \int_0^1 \xi_{ts,\varphi}(0,\delta)\,d\mu \quad (30)$$

where the first term on the right hand side is the radiation from the wall-layer and the second term is the one from the core. The radiation that reaches the core is the sum of the integrated radiative fluxes from the furnace walls and the FBL.

$$Q_{rad,out} = 4D \int_{H_0}^{H} \left(E_+(\delta,z) + 2J(z) \int_0^1 \xi_{ts,\varphi}(0,\delta)\mu\,d\mu \right) dz. \quad (31)$$

The radiative heat transfer coefficient is expressed in analogy to the convective one

$$\alpha_{rad} = (Q_{rad,in} - Q_{rad,out})/(4D(H-H_0)(T_c - T_w)). \quad (32)$$

Assuming the radiative and convective coefficient to be additive, the total heat transfer coefficient becomes

$$\alpha_{tot} = \alpha_{conv} + \alpha_{rad}. \quad (33)$$

To use the heat balance, the various quantities needed, K, $\psi(H)$, b_i, η, δ, T_c and a_i, have to be determined by empirical information.

SENSITIVITY OF THE MODEL

Influences on the heat balance will be investigated in two steps: first the assumptions will be discussed, then the effects of uncertainties in parameters will be analyzed.

Assumptions and approximations

The heat balance is carried out for steady-state conditions. Rapid fluctuations in particle concentration and temperature are not considered important. The influence of the gas phase is neglected, since its heat capacity is much lower than that of the particles.

There is a certain difference in bed particle size in the bottom part of the bed and in the upper parts where the heat transfer surfaces are situated [3]. As will be shown below, this has a small influence. Furthermore, a Sauter mean diameter, which is used in the calculations, is a good representation, since it gives the same projected particle area as the corresponding size distribution.

Measurements [18] have shown about two times higher downward particle flux in the vertical corners of the furnace than in the central parts of the walls, but this effect is limited to a rather small area, and therefore corner effects can be neglected. The membrane tube configuration results in higher particle concentrations in the region between the fins than on the crests of the tubes, but this can be represented by an average flux toward a projected surface [18]. It has been shown [14, 19] that the transversal distribution of particle concentration $\gamma(x)$ is almost independent of height in the transport zone and similar to results from other CFB risers.

A weakness of the description is that only the net horizontal particle transfer is accounted for. A separation of in-flow and out-flow of particles in the FBL would result in a higher heat transfer, since the outflowing particles are colder. Measurements in a laboratory CFB [20] shows that the in-flow and the outflow are about the same at a height of $z/D \approx 40$. The net flow was directed to the core in the upper part of the riser, at $z/D > 40$ and to the wall-layer in the lower part, at $z/D < 10$. The corresponding axial profile of particle concentration was decreasing with height for $z/D < 10$, is then constant until $z/D \approx 40$ where it started to increase slightly towards the top. Utility size CFB combustors have $H/D < 10$, which corresponds to the lower part of the laboratory CFB used in Ref. [20]. The particle concentration decreases all the way up through the combustion chamber and this supports the assumption that the in-flow to the wall-layer dominates over the out-flow. In such a situation the wall-layers are being filled with particles.

Heat generation by combustion in the FBL was neglected. An estimate of the influence of combustion flow that 30% of the bed particles are between H_0 and H at full load, and one third of this quantity may be in the FBL. During coal combustion an average fuel concentration in the transport zone may be 2 and 4% in the bottom bed (L. E. Åmand, private communication). The part of char particles in the FBL is therefore at most 5% of the fuel particles in the furnace ($0.3 \times 0.33 \times 0.02/(0.3 \times 0.02 + 0.7 \times 0.04) \approx 5\%$). About 50% of the heat is extracted through the membrane walls, and hence the error due to combustion in the FBL cannot be more than 10%. Actually, the error must be even less, because the low temperature in the FBL gives a very low rate of combustion. It is therefore reasonable to neglect this heat source.

The assumption of a constant horizontal temperature profile for loads above about 50% is supported by many measurements, such as those presented in Fig. 3 or Ref. [1]. Some measurements show an influence of height [21], but the variations are not much larger than those illustrated in Fig. 3. It would be possible to include a variable temperature profile if the variations were significant. The use of a constant particle velocity in the FBL, while calculating the cup mixing temperature, is based on the few measurements available [22, 23].

The core was assumed to be optically thick and no influence of radiation from surrounding walls was accounted for. The lowest cross-section average particle concentration during the tests was 0.04% in the CUT boiler yielding an optical depth of about 2.5 [eqn (24)]. Figure A1 shows that this optical depth is

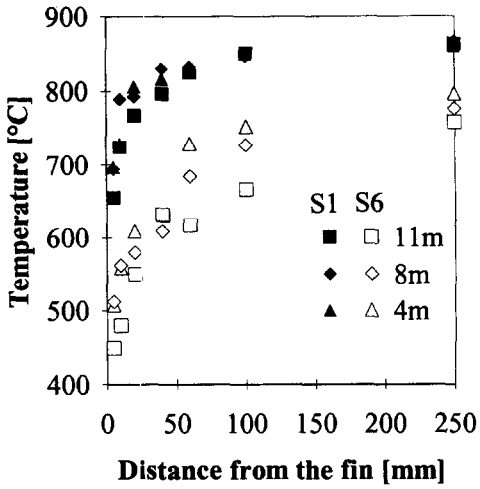

Fig. 3. Transversal temperature profiles at different heights above the air distributor. The data for the cases S1 and S6 are given in Table 1.

sufficient to consider the core optically thick in all cases studied.

In summary, the only assumption that may have essentially influenced the results is the one concerning the horizontal in-flow and out-flow of particles from the FBL. This assumption has to be further investigated.

Error analysis

The influence of errors in the parameters was investigated by means of sensitivity indices, which relate the error of the calculated HTC to those of the parameters. It could be concluded that the convective component is sensitive to the thickness of the FBL, δ, to parameters that describe the vertical particle concentration profile, K and $\psi(H)$, and to the temperature, T_c and a_i. A relative error in one of these factors produced a relative error of the same magnitude in the computed HTC. Other parameters did not significantly influence the convective HTC. The radiative heat transfer component was stable vs all parameters and the maximum error will therefore only be estimated for the convective component.

With some approximation the convective heat transfer coefficient is proportional to the product of the temperature difference between core and FBL, the decay constant and the mass of particles in the transport zone,

$$\alpha_{conv} \propto (T_c - T_{cup}) Km. \tag{34}$$

The relative deviation is obtained by differentiation and division by the original expression,

$$\Delta\alpha_{conv}/\alpha_{conv} = \Delta(T_c - T_{cup})/(T_c - T_{cup}) + \Delta K/K + \Delta m/m \tag{35}$$

and the maximum error in the convective component is estimated by adding the relative errors.

EXPERIMENTAL DATA

Experimental information is needed for the calculation. Some data are available from correlations, but other properties are not generalized and measured data for the specific case are needed.

The thickness of the wall-layer, δ, is defined as the distance where particles move downwards. Data from several CFBs were investigated in Ref. [22]. The thickness was found to increase slightly within a few diameters from the top. The data was summarized by a height independent correlation,

$$\delta = 0.05 \cdot D^{0.74}. \tag{36}$$

A correlation for the horizontal particle distribution in risers with $D < 0.3$ m [24] was later shown to be valid also for large boilers [14]. Equation (4) fitted to the data of Ref. [24] gives the coefficients: $b_0 = 0.3$, $b_1 = 3$ and $b_2 = 15$. The error analysis showed that the estimated HTCs were rather insensitive to the value of these parameters.

Data on emissivities of particles forming the bed material in CFB furnaces range from 0.4 to 0.85 [1, 25, 26, 27] and a value of $\varepsilon_p = 0.6$ is used in this work. The gas emissivity, calculated with eqn (22), is about 0.23.

The remaining properties, transversal temperature profile in the wall layer and the axial particle concentration profile, need to be measured. These data, as well as heat transfer to the wall, are available for three boilers: the 12 MWth boiler at Chalmers University of Technology, CUT (described in Ref. [28]), the 72 MWth Chatham boiler [29, 30], and the 109 MWth Flensburg boiler [1, 31]. The data and the geometry of these boilers are presented in Table 1.

The temperature profiles in the boundary layer of the Chalmers boiler were measured with a radiation shielded thermocouple, as described in Ref. [32]. The temperatures in two cases are shown in Fig. 3. The temperature profiles are independent of height at a given fluidization velocity. There is, however, a tendency for the temperatures to decrease with increasing height, at least at the lower fluidization velocity. The temperatures in the Chatham boiler were measured by an unshielded thermocouple [30], and in the Flensburg boiler by a thermocouple with a U-shaped shield [1], minimizing the radiative exchange with the wall but not with the core. The transversal temperature profiles are fitted to eqn (14). The maximum uncertainty in the temperature measurement in the CUT boiler was ± 25°C due to radiative exchange and ± 15°C due to natural fluctuations in the boiler. The sum of these uncertainties corresponds to about 20% of the temperature difference between the core and the FBL.

The cross-sectional average suspension densities were obtained from the measured vertical pressure drop. In particular the gradient of the vertical density profile is needed for the determination of the transversal mass-flow, eqn (11). The gradient is fairly small in the transport zone and this makes the curve-fit by eqn (3) sensitive to uncertainties in measurements. In the CUT boiler, 15 differential pressures were mea-

Table 1. Geometrical and experimental input to the heat balance

Case	Boiler	D [m]	H [m]	H_0 [m]	K† [m^{-1}]	$\psi(H)$ [%]	k [m/s]	η	T_w [°C]	T_c [°C]	a_1 [°C]	a_2	u [$m\ s^{-1}$]	d_p [μm]
S1	CUT	1.7	13.5	2	0.20	0.154	0.22‡	0.4	215	860	180	50	4.6	320
S2	CUT	1.7	13.5	2	0.18	0.058	0.11‡	0.4	215	850	200	30	3.5	320
S3	CUT	1.7	13.5	2	0.15	0.058	0	0.4	215	770	325	25	1.8	320
S5	CUT	1.7	13.5	2	0.20	0.115	0.14‡	0.4	215	820	200	40	2.7	200
S6	CUT	1.7	13.5	2	0.15	0.077	0.03‡	0.4	215	790	300	30	1.5	200
Ch	Chath	4.0	23	10	0.17	0.077	0.15§	0.3	280	875	110	35	6.4	200¶
F	Flensb	5.1	28	12	0.13	0.115	0.23§	0	340	855	240	80	6.3	220

† From curve fit of eqn (3).
‡ From eqn (11).
§ From particle flux measurements [15].
¶ Estimated from a particle size distribution of a similar case at the same boiler.

sured in the transport zone with a precision which was estimated by adding all differential pressures and comparing with an independently measured total pressure drop. The difference was less than 15%, but scatter in the measured pressure drops causes a standard deviation of 35% in the fitted decay constant. In the Chatham boiler the pressure was measured in five positions yielding four differential pressures, and in the Flensburg boiler seven pressures were measured in the transport zone. In these cases the errors may be considerable due to insufficient data. In order to improve the data, net transport coefficients were calculated from measured axial mass-fluxes [15]. In lack of measured profiles a correlation based on limited data has been presented for the decay constant [15],

$$K = 0.23/(u - v_t). \tag{37}$$

RESULTS

The wall average heat transfer coefficients based on the projected wall area and its radiative and convective constituents are calculated for the conditions given in Table 1. The calculated coefficients are compared with the corresponding measured ones in Fig. 4(a). The deviation between measured and calculated values does not exceed 40%, the calculated values being on average 25% lower than the measured ones in the CUT boiler.

The wall average radiative component clearly decreases with increased suspension density, Fig. 4(b), and the convective component increases significantly with suspension density.

The relative maximum uncertainty in the temperature difference is about 20%, in the decay constant 35% and in the mass of particles in the transport zone 15%. This gives a maximum uncertainty in the convective heat transfer coefficient of about 70%, according to eqn (35). The uncertainty of the determination of the radiative component is much lower, as seen in Fig. 4(b), and the maximum uncertainty of the total heat transfer coefficient is below 50%.

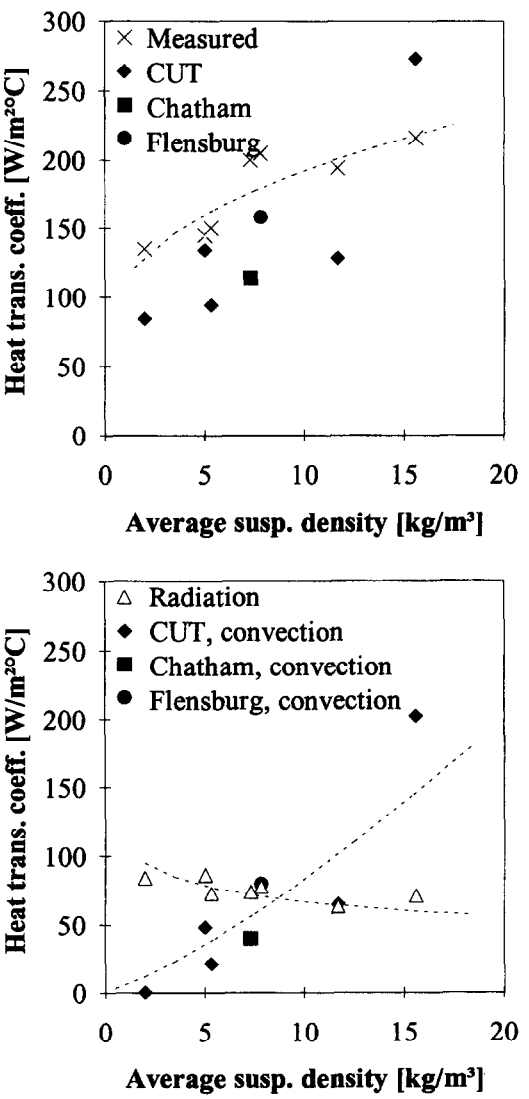

Fig. 4. (a) Measured and calculated total wall average heat transfer coefficients. The dotted line connects the measured values from the various plants. (b) Corresponding calculated radiative and convective heat transfer coefficients. The dotted lines connect the calculated values.

DISCUSSION

The basic idea of the model presented is that heat is transported by particles from the core of the transport zone, where combustion takes place, to the descending particle layers at the walls and further to the heat transfer surfaces forming the walls of the transport zone. A radiative transport of heat is added. The supply of particles to the FBL comes from the observed decay of particle concentration in the upward direction, as described by the decay constant and its related quantity, the net deposition coefficient. As long as a considerable decay takes place and all backmixing takes place in the FBL, it can be assumed that the supply of particles to the FBL dominates greatly over the particle flow leaving the FBL. Although this assumption has not been directly quantified, it is based on available observations from wide ducts, such as those of combustion chambers, in contrast to tall and narrow ducts, where an equilibrium can be attained after a certain fraction of riser height (at a normally large total height–diameter ratio). Under equilibrium conditions the flows of particles in and out of the boundary layer are equal by definition.

The estimation of the radiative transfer was shown to be relatively reliable. In extreme cases, for a transparent and an optically thick FBL, calculated radiative heat transfer coefficients are about 100 and 50 W m^{-2} $°C^{-1}$, respectively [33]. The two cases correspond to a low and a high suspension density and agree fairly well with the wall average data presented in Fig. 4(b).

The calculated and measured total heat transfer coefficients never deviate more than 40%, but the tendency is that the calculated values are lower than the measured ones. This agrees rather well with the analysis of maximum errors, indicating that the determination of the decay constant has to be improved. Pressure drop profiles measured with good resolution, good precision and low scatter are required.

The temperature in the core of the three boilers investigated ranged from 850 to 870°C and the wall layer temperature from 600 to 700°C. The maximum temperature fall was 270°C and the smallest was 150°C, or approximately 200 ± 50°C. This uncertainty should be compared with an estimated maximum uncertainty in the temperature measurements of 40°C. The predicted heat transfer at full load using a standard temperature profile, e.g. [1], is therefore almost as reliable as if a measured temperature profile was used. The temperature profile in the FBL is a product of the heat transfer through the FBL and the profile ought to be calculated by a model that describes this heat transfer process.

When judging the magnitudes of errors and deviations it should be borne in mind that the experimental data are obtained from commercial-size CFB boilers. This limits the amount of measurements in the tests quoted. On the other hand these tests are the only ones published until now.

CONCLUSIONS

The heat balance presented is based on a time-average fluid-dynamic model of core-annulus type, and gives the average heat transfer to the entire heat receiving wall. The particle convective heat transfer originates from a horizontal particle flow, which is also the reason for the vertical decay of particle concentration in the transport zone. An additive radiative component from the particulate medium was calculated by a continuum approach. An investigation of the reliability of the heat balance shows that the only assumption that may have an essential influence is the use of a horizontal net flow of particles, instead of an in-flow and an out-flow of particles from the wall-layer.

A measured vertical particle concentration profile and transversal temperature profiles are needed to calculate the heat transfer to the walls. This information is available for three commercial-size CFB boilers. Calculated and measured heat transfer coefficients deviate less than 40% and the calculated is on average 25% lower than measured ones. The maximum error was found to be less than 50% and was due to uncertainties in the measured data. To improve the accuracy of the prediction, it is most important to determine the decay coefficient from pressure drop profiles with good resolution and low scatter.

REFERENCES

1. Werdermann, C. and Werther, J., Heat transfer in large-scale circulating fluidized bed combustors of different size. In *Circulating Fluidized Bed Technology IV*, ed. A. A. Avidan, AIChE, 1994, pp. 428–435.
2. Wirth, K.-E., Heat transfer in circulating fluidized beds. *Chemical Engineering Science*, 1995, **50,** 2137–2151.
3. Andersson, B.-Å., Effects of bed particle size on heat transfer in CFB-Boilers. *Powder Technology*, 1996, **87,** 239–248.
4. Basu, P., Heat transfer in high temperature fast fluidized beds. *Chemical Engineering Science*, 1990, **45,** 3123–3136.
5. Wu, R. L., Grace, J. R. and Lim, C. J., Model for heat transfer in circulating fluidized beds. *Chemical Engineering Science*, 1990, **45,** 3389–3398.
6. Lints, M. L. and Glicksman, L. R., Parameters governing particle-to-wall heat transfer in a circulating fluidized bed. In *Circulating Fluidized Bed Technology IV*, ed. A. A. Avidan, AIChE, 1994, pp. 350–355.
7. Fang, Z. H., Grace, J. R. and Lim, C. L., Local particle convective heat transfer along surfaces in circulating fluidized beds. *International Journal of Heat and Mass Transfer*, 1995, **38,** 1217–1224.
8. Lints, M. L. and Glicksman, L. R., The structure of particle clusters near the wall of a circulating fluidized bed. *AIChE Symposium Series*, 1993, **89**(296), 35–52.
9. Johnsson, F., Zhang, W., Johnsson, H. and Leckner, B., Optical and momentum probe measurements in a CFB furnace. *Preprints of the Fifth International Conference on Circulating Fluidized Beds*, Institute of Chemical Metallurgy, Beijing, 1996, pp. M17 : 1–6.
10. Wu, R. L., Lim, C. J., Grace, J. R. and Brereton, C. M. H., Instantaneous local heat transfer and hydrodynamics in a circulating fluidized bed. *International Journal of Heat and Mass Transfer*, 1991, **34,** 2019–2027.

11. Wirth, K.-E., Seiter, M. and Molerus, O., Concentration and velocity of solids in areas close to the walls in circulating fluidized bed systems. *VGB Kraftwerkstechnik*, 1991, **10,** 824–828.
12. Johnsson, F. and Leckner, B., Vertical distribution of solids in a CFB-furnace. *Proceedings of the Thirteenth International Conference on Fluidized Bed Combustion*, Vol. 1, ASME, New York, 1995, pp. 671–679.
13. Schaub, G., Reimert, R. and Albrecht, J., Investigation of emission rates from large scale CFB-combustion plants. *Proceedings of the Tenth International Conference on Fluidized Bed Combustion*, ASME, San Francisco, 1989, pp. 685–691.
14. Zhang, W., Johnsson, F. and Leckner, B., Characteristics of the lateral particle distribution in circulating fluidized bed boilers. In *Circulating Fluidized Bed Technology IV*, ed. A. A. Avidan, AIChE, 1994, pp. 266–273.
15. Johnsson, F., Zhang, W. and Leckner, B., Characteristics of the formation of particle wall-layers in CFB boilers. *Proceedings of the Second International Conference on Multiphase Flow*, The Japan Society of Multiphase Flow, Nagoya, 1995, pp. FB1.25–FB1.32.
16. Bolton, L. W. and Davidsson, J. F., Recirculation of particles in fast fluidized bed. In *Circulating Fluidized Bed Technology II*, ed. P. Basu and J. F. Large, Pergamon Press, Oxford, 1988, pp. 139–146.
17. Leckner, B., Spectral and total emissivity of water vapor and carbon dioxide. *Combustion and Flame*, 1972, **19,** 33–48.
18. Zhang, W., Fluid dynamics of the transport zone of circulating fluidized beds—with application to boilers. Ph.D. thesis, Chalmers University of Technology, Gothenburg, 1995.
19. Beaud, F. and Louge, M., Similarity of radial profiles of particle volume fraction in a circulating fluidized bed. In *Fluidization VIII*, ed. J. F. Large and C. Laguérie, Engineering Foundation, New York, 1997, pp. 245–253.
20. Zhou, J., Grace, J. R., Lim, C. J., Brereton, C. H. M., Qin, S. and Lim, K. S., Particle cross-flow, lateral momentum flux and lateral velocity in a circulating fluidized bed. *Canadian Journal of Chemical Engineering*, 1995, **73,** 612–619.
21. Golriz, M. R., An experimental correlation for temperature distribution at the membrane tube wall of CFB boilers. *Proceedings of the Thirteenth International Conference on Fluidized Bed Combustion*, Vol. 1, ASME, New York, 1995, pp. 499–505.
22. Zhang, W., Johnsson, F. and Leckner, B., Fluid-dynamic boundary layers in CFB boilers. *Chemical Engineering Science*, 1995, **50,** 201–210.
23. Koeningsdorff, R. and Werther, J., Gas-solid mixing and flow structure modeling in the upper part dilute zone of a circulating fluidized bed. *Powder Technology*, 1995, **82,** 317–329.
24. Zhang, W., Tung, Y. and Johnsson, F., Radial voidage profiles in fast fluidized beds of different diameters. *Chemical Engineering Science*, 1991, **46,** 3045–3052.
25. Grace, J. R., Heat transfer in circulating fluidized beds. In *Circulating Fluidized Bed Technology*, ed. P. Basu, Pergamon Press, Toronto, 1986, pp. 63–80.
26. Steward, F. R., Couturier, M. F. and Poolpol, S., Analysis for radiative heat transfer in a circulating fluidized bed. *Proceedings of the Thirteenth International Conference on Fluidized Bed Combustion*, ASME, New York, 1995, pp. 507–513.
27. Glatzer, A., Ein Model für Strahlungswärmeübergang in ziruklierenden Wirbelschichten. *BWK*, 1995, **47,** 43–48.
28. Leckner, B., Golriz, M. R., Zhang, W., Andersson, B.-Å. and Johnsson, F., Boundary layers—first measurements in the 12 MW CFB research plant at Chalmers University. *Proceedings of the Eleventh International Conference on Fluidized Bed Combustion*, ASME, New York, 1991, pp. 771–776.
29. Couturier, M. F., Doucette, B., Stevens, D., Poolpol, S. and Razbin, V., Temperature, gas concentration and solids mass flux profiles within a large circulating fluidized bed combustor. *Proceedings of the Eleventh International Conference on Fluidized Bed Combustion*, ASME, New York, 1991, pp. 107–114.
30. Couturier, M. F., Steward, F. R. and Poolpol, S., Experimental determination of heat transfer coefficient in a 72 MWth circulating fluidized bed boiler. *Proceedings of the Twelfth International Conference on Fluidized Bed Combustion*, ASME, New York, 1993, pp. 1215–1222.
31. Werdermann, C., Feststoffbewegung und Wärmeübergang in zirkulierenden Wirbelschichten von Kohlkraftwerken. Ph.D. thesis, Technische Universität Hamburg-Harburg, Hamburg, 1992.
32. Leckner, B. and Andersson, B.-Å., Characteristic features of heat transfer in circulating fluidized bed boilers. *Powder Technology*, 1992, **70,** 303–314.
33. Baskakov, A. P. and Leckner, B., Radiative heat transfer in circulating fluidized bed furnaces. *Powder Technology*, 1997, **90,** 213–218.
34. Modest, M. F., *Radiative Heat Transfer*. McGraw-Hill, New York, 1993, p. 491.
35. Andersson, K. G. and Böiers, L.-E., *Ordinära differentialekvationer*, Studentlitteratur, Lund, 1992, Chap. 2.
36. Levdanskii, V. V. and Leitsina, V. G., Computation of the radiation flux emanating from a highly dispersive layer. *Journal of Engineering Physics*, 1991, **59,** 1266–1272.
37. Hottel, H. C. and Sarofim, A. F., *Radiative Transfer*. McGraw-Hill, New York, 1967, pp. 413–415.

APPENDIX A: ESTIMATION OF THE EFFECTIVE EMISSIVITY OF A PARTICLE CLOUD BY THE TWO-FLUX MODEL

The radiation emitted by particles in a particle cloud may be scattered. The scattering makes the effective emissivity of the cloud different from the emissivity of the particles. The effective emissivity of an infinite plane parallel cloud is obtained by the two-flux approximation of radiative transfer, solved for a particle cloud with constant temperature and particle concentration.

By assuming isotropic radiation and average hemispheric attenuation, the equation of radiative transfer can be simplified to two coupled equations for the intensity in the forward and backward direction, I_+ and I_-, e.g. [34].

$$\frac{\mathrm{d}I_+(x)}{2C\,\mathrm{d}x} = -\left(\varepsilon_p + \frac{1-\varepsilon_p}{2}\right) I_+(x) + \frac{1-\varepsilon_p}{2} I_-(x) + \varepsilon_p I_b \quad \text{(A1a)}$$

$$\frac{\mathrm{d}I_-(x)}{2C\,\mathrm{d}x} = -\frac{1-\varepsilon_p}{2} I_+(x) + \left(\varepsilon_p + \frac{1-\varepsilon_p}{2}\right) I_-(x) - \varepsilon_p I_b \quad \text{(A1b)}$$

where C is the projected area of the particles in a unit volume with the volumetric particle concentration c.

$$C = 3c/2d_p. \quad \text{(A2)}$$

The terms on the right hand of eqn (A1a) correspond to absorption and in-scattering of the radiation in the forward direction, in-scattering of radiation in the backward direction and increase by emittance from the particles between x and $x+\mathrm{d}x$. The radiative inflow is put to zero at the boundaries in order to calculate the radiation generated in the slab

$$I_+(-\kappa/2) = I_-(\kappa/2) = 0. \quad \text{(A3)}$$

Due to the symmetry of the system of equations and the boundary conditions, there is also symmetry in the solution

$$I_+(x) = I_-(-x). \tag{A4}$$

For solution of the coupled system of equations it is written in matrix form.

$$\frac{\mathrm{d}}{\mathrm{d}x}\begin{bmatrix} I_+(x) \\ I_-(x) \end{bmatrix} = C\begin{bmatrix} -(1+\varepsilon_p)(1-\varepsilon_p) \\ -(1-\varepsilon_p)(1+\varepsilon_p) \end{bmatrix}\cdot\begin{bmatrix} I_+(x) \\ I_-(x) \end{bmatrix} + 2\begin{bmatrix} C\varepsilon_p I_b \\ -C\varepsilon_p I_b \end{bmatrix} = CAI(x)+s. \tag{A5}$$

The homogeneous solution to the system, $s = 0$, is given by

$$I_{hom}(x) = \exp[CAx]\cdot\begin{bmatrix} \beta_1 \\ \beta_2 \end{bmatrix} \tag{A6}$$

where β_1 and β_2 are coefficients, which are determined by the boundary conditions, eqn (A3). A particular solution can be obtained by

$$I_{part}(x) = \int_0^x \exp[CA(\zeta - x)]\cdot s\,\mathrm{d}\zeta. \tag{A7}$$

According to the Caley–Hamilton theorem, e.g. [35], the matrix exponent can be expressed as a polynomial including the exponent function of the eigenvalues of the matrix A, $\pm 2\varepsilon_p^{1/2}$.

$$\exp[CAx] = \frac{1}{4\varepsilon_p^{1/2}}\begin{bmatrix} -1+2\varepsilon_p^{1/2}-\varepsilon_p & 1-\varepsilon_p \\ -1+\varepsilon_p & 1+2\varepsilon_p^{1/2}+\varepsilon_p \end{bmatrix} \times \exp[2C\varepsilon_p^{1/2}x] + \frac{1}{4\varepsilon_p^{1/2}}\begin{bmatrix} -1-2\varepsilon_p^{1/2}-\varepsilon_p & 1-\varepsilon_p \\ -1+\varepsilon_p & 1-2\varepsilon_p^{1/2}+\varepsilon_p \end{bmatrix} \times \exp[-2C\varepsilon_p^{1/2}x]. \tag{A8}$$

The homogeneous solutions are obtained by combining eqns (A6) and (A8).

$$I_{+,hom}(x) = [(-1+2\varepsilon_p^{1/2}-\varepsilon_p)\beta_1 + (1-\varepsilon_p)\beta_2]\exp[2\varepsilon_p^{1/2}Cx]/4\varepsilon_p^{1/2} + [(1+2\varepsilon_p^{1/2}+\varepsilon_p)\beta_1 - (1-\varepsilon_p)\beta_2]\exp[-2\varepsilon_p^{1/2}Cx]/4\varepsilon_p^{1/2} \tag{A9a}$$

$$I_{-,hom}(x) = [(-1+\varepsilon_p)\beta_1 + (1+2\varepsilon_p^{1/2}+\varepsilon_p)\beta_2]\exp[2\varepsilon_p^{1/2}Cx]/4\varepsilon_p^{1/2} + [(1-\varepsilon_p)\beta_1 - (1-2\varepsilon_p^{1/2}+\varepsilon_p)\beta_2]\exp[-2\varepsilon_p^{1/2}Cx]/4\varepsilon_p^{1/2}. \tag{A9b}$$

Particular solutions are found after integration of eqn (A7)

$$I_{+,part}(x) = I_b[1-\tfrac{1}{2}(1-\varepsilon_p^{1/2})\exp[2\varepsilon_p^{1/2}Cx] - \tfrac{1}{2}(1+\varepsilon_p^{1/2})\exp[-2\varepsilon_p^{1/2}Cx]] \tag{A10a}$$

$$I_{-,part}(x) = I_b[1-\tfrac{1}{2}(1+\varepsilon_p^{1/2})\exp[2\varepsilon_p^{1/2}Cx] - \tfrac{1}{2}(1-\varepsilon_p^{1/2})\exp[-2\varepsilon_p^{1/2}Cx]]. \tag{A10b}$$

The solution has to be symmetric, and since the particular solution is symmetric, this condition has to be fulfilled also for the homogeneous solution. Identification of the expressions in front of the exponential functions in the homogeneous solution gives

$$(-1+2\varepsilon_p^{1/2}-\varepsilon_p)\beta_1 + (1-\varepsilon_p)\beta_2 = (1-\varepsilon_p)\beta_1 - (1-2\varepsilon_p^{1/2}+\varepsilon_p)\beta_2 \tag{A11a}$$

$$(1+2\varepsilon_p^{1/2}+\varepsilon_p)\beta_1 - (1-\varepsilon_p)\beta_2 = -(1-\varepsilon_p)\beta_1 + (1+2\varepsilon_p^{1/2}+\varepsilon_p)\beta_2. \tag{A11b}$$

Both eqns (A11a) and (A11b) give $\beta_2 = \beta_1$. The relation between the integration constants is introduced in to the first part of the homogeneous solution, eqn (A9a), which is added to the corresponding particular solution, eqn (A10a), to get the total solution

$$I_+(x) = \frac{(1-\varepsilon_p^{1/2})(\beta_1 - I_b)\exp[2\varepsilon_p^{1/2}Cx]}{2} + \frac{(1+\varepsilon_p^{1/2})(\beta_1 - I_b)\exp[-2\varepsilon_p^{1/2}Cx]}{2} + I_b. \tag{A12}$$

Applying the first boundary condition, eqn (A3), gives an expression for β_1.

$$\beta_1 = I_b\left[1 - \frac{2}{(1+\varepsilon_p^{1/2})\exp[\varepsilon_p^{1/2}C\kappa] + (1-\varepsilon_p^{1/2})\exp[-\varepsilon_p^{1/2}C\kappa]}\right]. \tag{A13}$$

The objective of this appendix is to obtain an expression for the effective emissivity, which is defined as

$$\varepsilon_{eff} = I_+(\kappa/2)/I_b. \tag{A14}$$

Combination of eqns (A12) to (A14) gives

$$\varepsilon_{eff} = 2\sqrt{\varepsilon_p}\,\frac{\exp[\varepsilon_p^{1/2}C\kappa] - \exp[-\varepsilon_p^{1/2}C\kappa]}{(1+\varepsilon_p^{1/2})\exp[\varepsilon_p^{1/2}C\kappa] + (1-\varepsilon_p^{1/2})\exp[-\varepsilon_p^{1/2}C\kappa]}. \tag{A15}$$

Extend the fraction by $\exp[-\varepsilon_p^{1/2}C\kappa]$.

$$\varepsilon_{eff} = 2\varepsilon_p^{1/2}\,\frac{1-\exp[-2\varepsilon_p^{1/2}C\kappa]}{1+\varepsilon_p^{1/2}+(1-\varepsilon_p^{1/2})\exp[-2\varepsilon_p^{1/2}C\kappa]}. \tag{A16}$$

Discussion

From a model which assumes randomly moving photons in a porous medium of randomly distributed mono-sized opaque spheres [36] the effective emissivity for a particle concentration of 10% was computed and an expression for the effective emissivity of an optically infinite particle layer was derived,

$$\varepsilon_{eff}(\kappa \to \infty) = c\varepsilon_p + 2(1-c)\varepsilon_p^{1/2}/(1+\varepsilon_p^{1/2}). \tag{A17}$$

The corresponding asymptotic value of eqn (A16) for a large optical depth is

$$\varepsilon_{eff}(\kappa \to \infty) = 2\varepsilon_p^{1/2}/(1+\varepsilon_p^{1/2}). \tag{A18}$$

Equation (A17) shows a dependence on the particle concentration, c, but for suspensions as disperse as the one in the transport zone of a CFB furnace, the influence of particle concentration in eqn (A17) is negligible and eqns (A18)

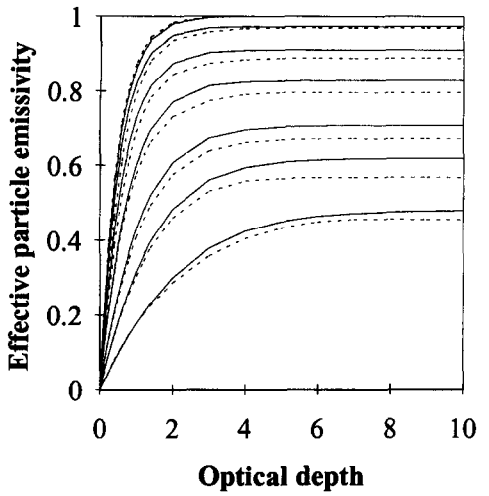

Fig. A1. The effective emissivity of a particle cloud calculated by eqn (A16), solid line, and according to Ref. [36], dashed line. The curves correspond to different particle emissivities, from the top; 1.0, 0.9, 0.7, 0.5, 0.3, 0.2 and 0.1.

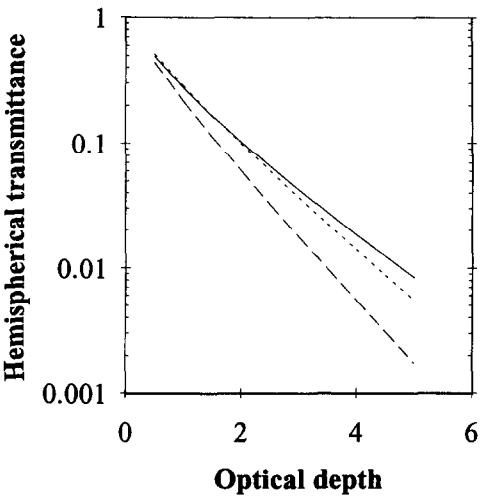

Fig. B1. Hemispherical transmittance for different simplifications of scattering; single-scattering, solid line; two-way scattering, dotted line and direct transmittance without scattering, dashed line. The emissivity of the particles is 0.6.

and (A17) are identical. In Fig. A1 the computed effective emissivities in Ref. [36] and values obtained from eqn (A16) are plotted as a function of the optical depth. The figure shows that the two models agree fairly well for all optical depths, but eqn (A16) gives slightly higher effective emissivities. This is due to the dependence of the particle concentration, as seen in eqn (A17).

Similar expressions for the effective particle emissivity were investigated [33] and all of them were in fair agreement with Ref. [36]. In conclusion, for the particle concentrations considered, the simplified expression, (A16), can be used.

APPENDIX B: SIMPLIFIED CALCULATIONS OF THE TRANSMITTANCE THROUGH A PARTICULATE MEDIUM

Radiation passing through a particulate medium is either directly transmitted through the medium, absorbed or scattered by the particles. The same applies for the scattered radiation, which can result in multiple scattering.

In a simplification [37] the transmittance is separated in direct transmittance and scattering transmittance, where multiple scattering is treated by two extreme cases. The direct transmittance, ξ_d, is the ratio of the directly transmitted and initial intensity. The attenuation of the direct radiation, I, in the direction φ in a slab of the thickness dx is proportional to the projected area of the particles per unit area.

$$-dI(x,\varphi) = I(x,\varphi)\frac{3}{2}\frac{c(x)}{d_p}\frac{dx}{\mu}, \tag{B1}$$

where $c(x)$ is the particle volume concentration and dx/μ is the distance through the slab. Integration of eqn (B1) from the horizontal position of the slab, x, to the border of the wall-layer, δ, gives the directional direct transmittance,

$$\xi_{d,\varphi}(x,\delta) = \exp\left[-\int_x^\delta \frac{3}{2}\frac{c(x)}{d_p}\frac{1}{\mu}dx\right]. \tag{B2}$$

Integration over the hemisphere gives the hemispherical transmittance, which is related to the emissive power of an isotropic source, in contrast to the directional transmittance, which is related to the intensity,

$$\xi_d(x,\delta) = 2\int_0^1 \exp\left[-\int_x^\delta \frac{3}{2}\frac{c(x)}{d_p}\frac{1}{\mu}dx\right]\mu\,d\mu. \tag{B3}$$

In order to calculate the scattering transmittance for a case of isotropic scattering, secondary scattering is assumed to be either totally absorbed or transmitted in the same direction as the primary one [37]. These extreme cases eliminate multiple scattering and gives a lower and upper limit of the transmittance and the latter extreme case is close to the real case of multiple scattering [37]. This single scattering approximation gives a possibility to investigate the influence of scattering on the total transmittance, which is the sum of the directional direct and scattering transmittances integrated over the hemisphere.

Also the single-scattering approximation is rather complicated to use, especially as the particle concentration is not constant. As a simplification, the scattering is assumed to be equal in the same or in the opposite direction of the emitted radiation, which gives a reduction of the intensity in analogy with eqn (B1).

$$-dI(x,\varphi) = I(x,\varphi)\left(\varepsilon_p + \frac{1-\varepsilon_p}{2}\right)\frac{3}{2}\frac{c(x)}{d_p}\frac{dx}{\mu}. \tag{B4}$$

The part ε_p of the attenuated radiation is absorbed and $(1-\varepsilon_p)/2$ is scattered in the backward direction. Integration over the distance from x to δ and over the hemisphere gives the hemispherical transmittance of the two-way scattering approximation in analogy with eqn (B3).

$$\xi_{ts}(x,\delta) = 2\int_0^1 \exp\left[-\int_x^\delta \frac{1+\varepsilon_p}{2}\frac{3}{2}\frac{c(x)}{d_p}\frac{1}{\mu}dx\right]\mu\,d\mu. \tag{B5}$$

The three methods; direct transmittance, ξ_d; single-scattering transmittance, ξ_{ss}; and two-way-scattering transmittance, ξ_{ts}, are compared for particle emissivities of 0.6 and constant particle concentration. The transmittances are plotted as a function of the optical depth, Fig. B1.

From Fig. B1 it can be concluded that the two-way scattering agrees fairly well with the single-scattering approximation, but the relative discrepancy grows larger as the optical depth increases. The discrepancy does not significantly affect the net transfer of radiation, since the absolute error is small compared to the net transfer and the two-way scattering approximation will therefore be used in the computation of the transmittance.